# Microscopic coupled-channels analysis of $^9$Be$(p,p')$ for $100 \leq E_p \leq 500$ MeV

J. J. Kelly
*Nationaal Instituut voor Kernfysica en Hoge Energiefysica (NIKHEF-K), Postbus 41882, 1009 DB Amsterdam, The Netherlands and Department of Physics, University of Maryland, College Park, Maryland 20742*
(Received 28 April 1992)

Microscopic coupled-channels calculations for the ground-state rotational band of $^9$Be are performed using the folding model and density-dependent effective interactions. Transition densities are obtained either from the shell model or from fits to electron scattering data. The quadrupole contribution to elastic scattering enhances the cross section and damps the analyzing power for momentum transfers larger than about 1.2 fm$^{-1}$. Channel coupling is more important for the $\frac{7}{2}^-$ than for the $\frac{5}{2}^-$ state and roughly follows the energy dependence of the interaction strength. Comparisons are made between calculations using either theoretical effective interactions or empirical effective interactions previously fitted to data for $^{16}$O or $^{40}$Ca. The results demonstrate that medium modifications are quite important and are well described by the local density approximation. Therefore, the effective interaction depends primarily upon local density and is almost independent of nucleus, state, or deformation.

PACS number(s): 24.10.Eq, 25.40.Cm, 25.40.Ep, 27.20.+n

## I. INTRODUCTION

The effective interaction for the scattering of 100–500 MeV protons has been shown to depend strongly upon the local density in the interaction region [1–7]. Qualitatively good descriptions of proton-nucleus scattering can be obtained using $G$ matrices computed for nuclear matter in conjunction with the local density approximation (LDA) [8–10]. More accurate results are obtained when the density dependence of the effective interaction is adjusted to reproduce elastic and inelastic scattering data for self-conjugate targets, for which measurements of the transition densities by electron scattering minimize ambiguities due to nuclear structure [11]. By including several states with transition densities of either interior or surface character the dependence upon density can be obtained with little ambiguity. We have shown that empirical effective interactions that are independent of both state and target can be obtained for ranges of energy and mass at least as large as $E_p = 100$–650 MeV and $A = 16$–40 [3–7, 11]. By comparing the interactions fitted to data for several targets, either independently or simultaneously, the hypothesis that local properties of finite nuclei are the same as those for infinite nuclear matter of corresponding density is tested independently of the accuracy of calculations made using nuclear matter theory. This is important because the substantial differences between the various nuclear matter calculations that are presently available are larger than would be expected from the differences among the nucleon-nucleon potentials that are used and probably reflect differences among the various untested approximation schemes.

Several difficulties might be encountered when attempting to extend this model to smaller nuclei. The assumption that medium modifications of the effective interaction are the same for small nuclei as for infinite nuclear matter with the local density becomes suspect for small targets. This assumption is expected to overestimate the importance of Pauli blocking, which is the dominant medium modification for low energies. Furthermore, the ambiguity in selecting the local density for a finite-range interaction becomes more important for small targets without a region of constant density. Finally, many $p$-shell nuclei are severely deformed, which exacerbates the ambiguities in the LDA hypothesis and leads to rotational bands with potentially strong channel coupling.

Therefore, we shall probe the limits of the LDA by analyzing proton scattering for the rotational band of $^9$Be in the energy range $E_p = 100$–500 MeV, a range for which extensive data exist. We have already demonstrated that the quadrupole deformation has important effects upon elastic scattering from $^9$Be at $E_p = 135$–180 MeV [12, 13], substantially increasing the cross section and dramatically damping the analyzing power for $q > 1.5$ fm$^{-1}$. In those analyses the elastic quadrupole contribution was computed in the distorted wave approximation, but the coupling to other members of the rotational band was neglected. Similar results at $E_p = 200$ MeV have been reported for $^{6,7}$Li by Glover *et al.* [14, 15] and for $^{10}$B by Lewis *et al.* [16]. In the present work we extend the model to include full coupled-channels calculations within the ground-state rotational band using microscopic potentials obtained from the folding model.

Traditional analyses of proton scattering by deformed nuclei are usually made in the symmetric rotor model assuming that the optical potential can be represented by the Woods-Saxon model and that the multipole poten-

 

tials can all be projected from the same deformed optical potential [17, 18]. This model was used by Roy *et al.* [19] to analyze the scattering 220 MeV protons by $^9$Be. However, neither the density distribution nor the optical potential for light nuclei can be adequately represented by simple Woods-Saxon shapes. Nor can the relationship between elastic and inelastic potentials be adequately represented by multipole projection from a common deformed potential. Finally, since the model contains many parameters, phenomenological analysis of the data is plagued by ambiguities and is prone to producing physically unreasonable parameter sets, particularly for light nuclei where the model is not really applicable anyway.

Several microscopic coupled-channels calculations have been reported in recent years. For example, Nesterenko *et al.* [20] analyzed $^{168}$Er$(p,p')$ at $E_p = 65$ MeV using a hybrid model in which the real parts of some of the central transition potentials were computed by folding random phase approximation (RPA) transition densities with the density-independent M3Y interaction of Bertsch *et al.* [21], whereas the remaining potentials were obtained from an asymmetric rotor model based upon phenomenological Woods-Saxon potentials. Similarly, Zalmstra, Harakeh, and Hienen [22] analyzed $^{28}$Si$(p,p')$ at $E_p = 65$ MeV using the density-dependent central strength of the JLM interaction of Jeukenne, Lejeune, and Mahaux [23], assuming a Gaussian shape, supplemented by phenomenological spin-orbit potentials. This hybrid interaction was folded with transition densities either from the symmetric rotor model or from the shell model. However, these *ad hoc* interaction models cannot be considered too reliable. Furthermore, the transition densities used in those calculations were not compared with electroexcitation measurements and may not be reliable either. Therefore, it is difficult to interpret the comparison between those calculations and their data. Use of the carefully calibrated interactions available for proton energies above 100 MeV and of measured transition densities should give more reliable and interpretable results.

In the present work we report microscopic coupled-channels calculations based upon density-dependent effective interactions. The present analysis is parameter-free in the sense that the effective interactions were previously calibrated to data for other nuclei and the form factors are determined by electromagnetic data whenever it is available. The nuclear structure amplitudes which cannot be calibrated against electromagnetic data were obtained from the shell model and are small anyway. In addition to the dominant $C2$ transition potentials, we also include the $M1$ and $M3$ amplitudes. Hence, these results represent the most complete microscopic coupled-channels calculations reported to date. No further parameters need to be adjusted to reproduce the data. These parameter-free calculations will be shown to describe the available data for energies above 100 MeV very well.

The data are discussed in Sec. II. A brief description of the model is presented in Sec. III. The sensitivity of the calculations to the difference between shell-model and electromagnetic form factors is studied in Sec. IV A, the importance of channel coupling in Sec. IV B, and medium modifications of the effective interaction in Sec. IV C. Our conclusions are summarized in Sec. V.

## II. EXPERIMENTAL DATA

The most complete experimental data on form factors within the rotational band of $^9$Be were obtained by Dixit *et al.* [13] using 180 MeV protons and by Glickman *et al.* [24] using electron scattering. By analyzing the variation of the position and width with momentum transfer, these authors were able to resolve the broad structure centered at an excitation energy of about 6.5 MeV into two peaks. By analyzing the form factors for these peaks, it was determined that the lower peak, at about 6.38 MeV, has a characteristic $C2$ angular distribution and should be identified as the $\frac{7}{2}^-$ member of the ground-state rotational band.

Proton quadrupole transition densities for the $\frac{3}{2}^- \rightarrow \frac{5}{2}^-$ and $\frac{3}{2}^- \rightarrow \frac{7}{2}^-$ transitions were extracted from the $(e,e')$ data by Glickman *et al.* [24]. Assuming that the $\frac{3}{2}^- \rightarrow \frac{3}{2}^-$ and $\frac{3}{2}^- \rightarrow \frac{5}{2}^-$ quadrupole form factors have the same shapes, the monopole form factor and the elastic quadrupole strength were also fitted. The transverse form factors give the strengths of the $M1$ and $M3$ form factors for the $\frac{3}{2}^-$ and $\frac{5}{2}^-$ states.

Neutron quadrupole transition densities were fitted to the $(p,p')$ data for the $\frac{5}{2}^-$ and $\frac{7}{2}^-$ states by Dixit *et al.* [13] assuming that a single multipole dominates and using the proton densities from Glickman *et al.* [24] as fixed input. The neutron density was virtually indistinguishable in shape from the proton density for the $\frac{5}{2}^-$ state, but a substantial difference was obtained for the $\frac{7}{2}^-$ state. Note that the coupling of the lower states to the $\frac{7}{2}^-$ state is sufficiently small that possible ambiguities in the extraction of the broad $\frac{7}{2}^-$ peak and resulting errors in its form factor do not materially affect the calculations for other states.

Additional proton scattering data for the $\frac{3}{2}^-$ and $\frac{5}{2}^-$ states are available for several energies between 100 and 500 MeV. These data were obtained using natural beryllium and BeO foils during experiments primarily designed to measure proton scattering from $^{16}$O. Data for some of the other states of $^9$Be are also available at some of these energies but are not considered herein. The data for 135 MeV were reported by Ref. [12] and analyzed using a preliminary version of the present model. The data for 100 and 200 MeV were acquired at the Indiana University Cyclotron Facility using the new K600 spectrometer. Details of the experiment and data analysis may be found in Ref. [25]. The unpublished data for 318 and 500 MeV were acquired at the Los Alamos Meson Physics Facility and are described in Ref. [26]. The accompanying data for $^{16}$O were reported in Refs. [6] and [7]. Finally, data for 220 MeV protons were acquired at TRIUMF and analyzed using the symmetric rotor model and deformed Woods-Saxon potentials by Roy *et al.* [19].

## III. MODELS

### A. Folding model

The dominant contributions to collective normal-parity transitions can be described by scattering potentials of the form

$$U_J(r) = U_J^Z(r) + U_J^C(r) + \nabla F_J^{LS}(r) \otimes \frac{1}{i}\nabla \cdot \sigma$$

where $U_J^Z$ is the Coulomb potential, $U_J^C$ is the central potential, and $F_J^{LS}$ is the spin-orbit potential for angular momentum transfer $J$. In the folding model the central and spin-orbit potentials

$$U_J^C(r) = \frac{2}{\pi}\int dq\, q^2 j_J(qr) \sum_\lambda \eta t_\lambda^C(q,\rho_0)\rho_{J\lambda}(q),$$

$$F_J^{LS}(r) = \frac{2}{\pi}\int dq\, q^2 j_J(qr) \sum_\lambda \eta \tau_\lambda^{LS}(q,\rho_0)\rho_{J\lambda}(q)$$

are obtained by convolution of the transition density $\rho_{J\lambda}$ with central and spin-orbit interactions $t_\lambda^C$ and $\tau_\lambda^{LS}$ where $\lambda$ denotes isospin and where $\eta$ is the Jacobian between $t$ matrices in the $NN$ and $NA$ frames. A local approximation to the exchange contribution is included within the definition of the effective interaction. For simplicity, the dependence of the effective interaction upon the local ground-state density $\rho_0(r)$ is evaluated at the site of the projectile.

Additional normal-parity contributions due to spin and current densities have been estimated in the shell model and found to be negligible. Small $M1$ and $M3$ multipole transitions were also computed using shell model densities, but their contributions to transitions within the rotational band are too small to merit inclusion of the relevant formulas. Further details on the folding model may be found in Refs. [27] and [14]. The coupled-channels calculations include all components of the nucleon-nucleon interaction except tensor exchange. The latter involves a complicated operator which is difficult to incorporate in the microscopic coupled-channels code, but first-order calculations demonstrate that tensor exchange is negligible for the present application.

The transition densities may be obtained from a nuclear structure model calibrated using electron scattering data. In the shell model the transition densities have the form

$$\rho_{J\lambda}^{fi}(r) = \sum_{ph} S_{J\lambda}^{fi}(p,h) R_p(r) R_h(r) \langle l_p j_p || Y_J || l_h j_h \rangle$$

where $fi$ denotes the transition between initial and final states, $p = (n_p l_p j_p)$ denotes the single-particle quantum numbers for a particle, $h = (n_h l_h j_h)$ denotes a hole, $S_{J\lambda}^{fi}(p,h)$ denotes the spectroscopic amplitude, and $R(r)$ denotes a single-particle radial wave function. The spectroscopic amplitudes for all intraband multipole transitions were obtained using the Cohen and Kurath 6-16 interaction [28, 24, 29]. For simplicity, oscillator wave functions with $b = 1.765$ fm were used and standard center-of-mass corrections were applied. Since it is well known that $p$-shell wave functions underestimate quadrupole effects, $C2$ effective charges $e_0 = 1.6$ and $e_1 = 0.7$ were used to reproduce the quadrupole moment. Furthermore, the magnetic multipoles were also renormalized to reproduce the $B(M\lambda)$ values obtained by Glickman *et al.* [24]. Although $(p,p')$ requires several transition densities not sampled by electron scattering, all densities for each multipole were scaled by the same factor. Hence, the $M1$ and $M3$ densities for the $\frac{3}{2}^-$ state were scaled by factors of 1.0 and 0.67 and for the $\frac{5}{2}^-$ state by 1.15 and 0.47. Transverse data are not available for the $\frac{7}{2}^-$ state. The shell model predictions for the remaining intraband transitions were included in all calculations without further modification. We identify this model of the transition densities as model 1.

Note that the use of Woods-Saxon radial wave functions similar to those used by Lewis *et al.* [16] for $^{10}$B do not improve the agreement between the shell model calculations and either the $(e,e')$ or $(p,p')$ data for $^9$Be. Those wave functions were based upon a fit made by Hicks *et al.* [30] to the $M3$ elastic form factor for $^{10}$B assuming a pure $1p_{3/2} \rightarrow 1p_{3/2}$ single-particle transition. However, it is well known that the single-particle radial wave functions which give the best fits to magnetic scattering do not also provide the best description of Coulombic multipole densities for light nuclei because core polarization is large and does not simply follow the valence density. In the absence of a microscopic model of core polarization it is better to use oscillator wave functions, adjusted to reproduce the rms charge radius, for the dominant $C2$ transition densities. Since the $M1$ and $M3$ contributions are much smaller, we use oscillator wave functions for all transition densities considered herein.

Alternatively, those transition densities that are directly measurable using electron scattering or proton scattering can be replaced with empirical densities. Proton quadrupole transition densities for direct transitions from the ground state were obtained by Glickman *et al.* [24], as described in Sec. II. The transverse form factors give the strengths of the $M1$ and $M3$ form factors for the $\frac{3}{2}^-$ and $\frac{5}{2}^-$ states. Neutron quadrupole transition densities were obtained by Dixit *et al.* [13]. For model 2 we use these empirical densities in conjunction with other transition densities computed within the shell model as described above.

We use density-dependent effective interactions either calculated using nuclear matter theory or fitted to proton scattering data for $A = 16$–$40$, as described in Refs. [2] and [11]. For $E_p < 200$ MeV we use the Paris-Hamburg $G$ matrix of von Geramb and collaborators [8, 9], but for $E_p \geq 200$ MeV we use the effective interaction constructed by Ray [10]. Both include Pauli blocking and binding effects, but the latter also includes pion production and intermediate isobar propagation and hence is more suitable for higher energies. These theoretical interactions are compared with the empirical effective interactions reported in Refs. [11, 4, 25, 6, 7]. Although several variations of the empirical effective interaction are available at each energy, the specific choices do not

affect the present results. Finally, we also consider calculations using the density-independent $t$ matrix of Franey and Love [31]. The Paris-Hamburg interaction is labeled as PH, the Ray interaction as LR, and the Franey-Love interaction as FL. Empirical effective interactions are labeled as EI.

The Cheon rearrangement factor [32, 33]

$$t(q,\rho)_{\text{inelastic}} = (1 + \rho\partial/\partial\rho)t_{\text{elastic}}(q,\rho)$$

was applied to all components of the effective interaction for inelastic scattering. This relationship effectively doubles the density dependence of the effective interaction for inelastic scattering with respect to the elastic interaction. We note that nuclear matter theory provides a model of the elastic interaction. Theoretical justification for this relationship has been given using either the collective model [32] or the hole-line expansion for nuclear matter [33]. Experimental justification for this relationship is found in the success of empirical effective interaction in fitting both elastic and inelastic scattering data simultaneously, which is not possible without a relationship of this form. Based upon the derivation of the rearrangement factor within the collective model, this factor was also applied to the $\Delta J > 0$ contributions to elastic scattering. Although the justification of this relationship is strongest for the normal-parity isoscalar components of the interaction, we have applied it to the other components also since those contributions are small within the rotational band anyway.

### B. Reaction model

The reaction code LEA [34] has been generalized to include coupled-channels calculations using algorithms based upon the Green function method of Raynal [18]. Two iteration procedures are available. The simplest is based upon straightforward expansion in powers of the coupling potentials such that each iteration is characterized by a uniform power of the coupling strength. Alternatively, the ECIS algorithm of Raynal continually incorporates contributions from stronger terms into the weaker terms, such that the greatest power of the coupling strength progressively increases within each stage of iteration. The former has the advantage that the first-order calculation is identical with the familiar distorted wave approximation, whereas the latter has the advantage of more rapid convergence. We have tested the code using the symmetric rotor model and obtain excellent agreement with the ECIS program [35]. For the folding model LEA includes several additional transition operators not included in ECIS.

We consider three variations of the reaction model. For elastic scattering we designate zeroth-order calculations based upon the spherical optical potential alone as OM for optical model. First-order calculations are designated as DWBA for distorted wave Born approximation. For elastic scattering the DWBA includes the $\Delta J = 1$, 2, and 3 contributions in the same manner previously used to analyze the data for 135 and 180 MeV. Full coupled-channels calculations using the ECIS iteration algorithm within LEA are designated as CC. All intraband transition potentials with $1 \leq \Delta J \leq 3$ were included. Both distorting and transition potentials were always generated from the same interactions self-consistently. For simplicity, the distorting potentials were independent of state.

## IV. RESULTS

In this section we examine the sensitivity of the results to various aspects of the model.

### A. Structure

The sensitivity of the 180 MeV data to the difference between theoretical and empirical $\Delta J = 0$ and $\Delta J = 2$ form factors is examined in Fig. 1. Full coupled-channels calculations were performed for both models described above, where the dashed curves are based on model 1 and the solid curves on model 2. The effect of the elastic $M3$ is only a few percent for $q \approx 1.5$ fm$^{-1}$ and is negligible elsewhere. The effect of the $M1$ multipole is negligible for the ground state and is appreciable for the $\frac{5}{2}^-$ state only for $q < 0.5$ fm$^{-1}$. Note that the present coupled-channels results are quite similar to the DWBA results

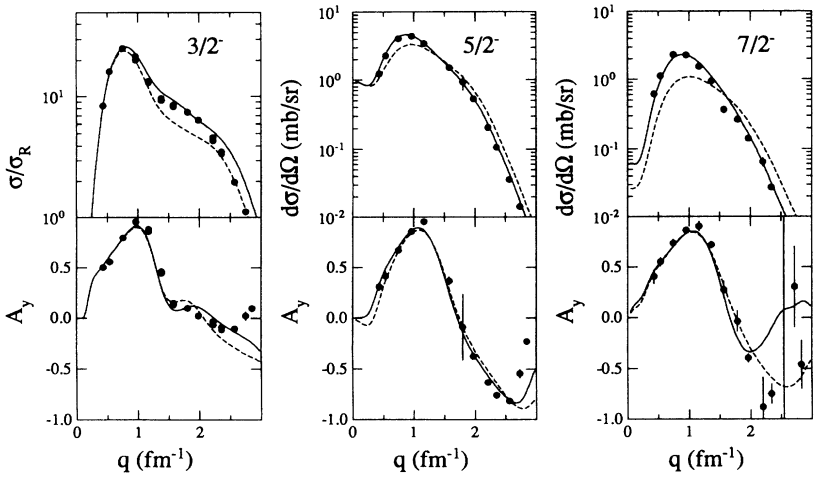


FIG. 1. Comparison of CC calculations for $^9$Be$(p,p')$ at $E_p = 180$ MeV using shell model or empirical transition densities. Dashed curves employ model 1 and solid curves model 2. See text for details. The elastic cross sections are presented as ratios to the Rutherford cross section $\sigma_R$ to enhance detail by suppressing several decades of range.

of Dixit *et al.* [13], except for a small enhancement of the quadrupole effect on elastic scattering, demonstrating that the first-order calculations remain quite accurate in this energy regime despite the large deformation of $^9$Be. This result justifies the Dixit procedure of fitting the inelastic transition densities to the data in DWBA assuming that only a single multipole contributes. Hence, we do not readjust any of the densities.

For the ground state we find that the stronger empirical quadrupole strength improves the agreement with the data for intermediate momentum transfers, $q \approx 1.5$ fm$^{-1}$. Similarly, the empirical densities give better agreement with the inelastic cross sections, especially for the $\frac{7}{2}^-$ state. The most important differerence between the two models of the $\frac{7}{2}^-$ state is found in the fit to the electromagnetic $C2$ form factor, with the difference between the experimental neutron and proton transition densities being relatively unimportant.

Nevertheless, small discrepancies remain between the elastic scattering calculations and the data. The calculated elastic cross sections are slightly too high for $q \approx 1.2$ fm$^{-1}$ and significantly too high for $q > 2.2$ fm$^{-1}$. Assuming that the interaction model is accurate, improved agreement with the data could be obtained by shifting the monopole form factor towards smaller momentum transfer. In the calculations we assumed, in the absence of better information, that the neutron and proton monopole densities share a common shape and are simply proportional. Since the threshold for neutron emission is only 1.665 MeV, it is reasonable to suppose that the neutron density might possess a significantly longer tail than the proton density. This effect could cause the monopole form factor to fall fast enough to reproduce the data.

However, there remain too many possible sources of ambiguity to justify fitting the monopole form factor to these data at this time. The quadrupole contribution to electron scattering obviates model-independent extraction of the proton monopole density and leads to appreciable uncertainty in the precise location of its minimum. Furthermore, the accuracy of the interaction model for light deformed nuclei has not yet been adequately established. Therefore, we resist the temptation to fit the data, preferring to present instead a parameter-free survey of the energy dependence of the reaction mechanism. The present level of accuracy gives us confidence that the nuclear structure is known well enough for that purpose.

### B. Reaction mechanism

Elastic and inelastic scattering calculations for 100, 200, 318, and 500 MeV are compared with the data in Figs. 2–4. Model 2 was used for the structure and empirical effective interactions were employed. The dotted curves represent DWBA calculations for which the intraband coupling is limited to first order only. The solid curves, labeled CC, represent full microscopic coupled-channels calculations for the rotational band. For elastic scattering two additional calculations are shown. The dashed curves represent OM calculations using only the spherical optical potential. Finally, the dash-dotted curves, labeled CC0, represent coupled-channels calculations for which only the ground state is included.

By comparing the elastic DWBA and CC0 calculations we can evaluate the accuracy of first-order calculations of elastic reorientation without coupling to excited states. For all energies we find that the first-order calculations are already quite accurate, confirming the essential validity of our earlier DWBA calculations for elastic scattering from $^9$Be. Iteration enhances the reorientation effect only slightly, but coupling to excited states has a larger effect upon elastic scattering for large momentum transfer than iteration of elastic reorientation.

Both the elastic and inelastic cross sections decrease in strength between 100 and 200 MeV and then increase between 200 and 500 MeV, roughly following the energy dependence of the spin and isospin independent component of the central interaction. Similarly, the differences between DWBA and CC calculations are qualitatively smallest near 200 MeV and also roughly follow the energy dependence of the interaction strength. Only near 100 MeV are the effects of channel coupling evident for small momentum transfers. Channel coupling enhances the effects upon elastic scattering for large momentum transfer and improves the agreement with the analyzing-

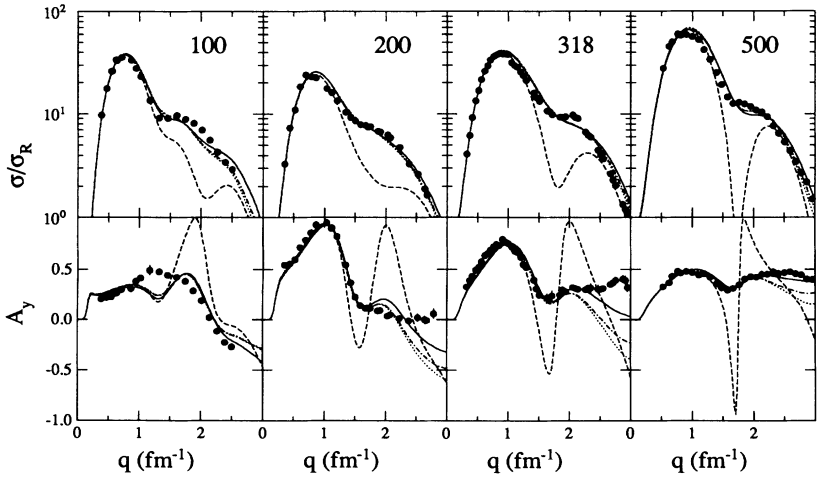


FIG. 2. Energy dependence of reaction models of $^9$Be$(p,p')\frac{3}{2}^-$ for $100 \leq E_p \leq 500$ MeV. Dashed curves portray OM calculations, dotted curves DWBA, dash-dotted CC0, and solid curves CC. Model 2 is used for transition densities.

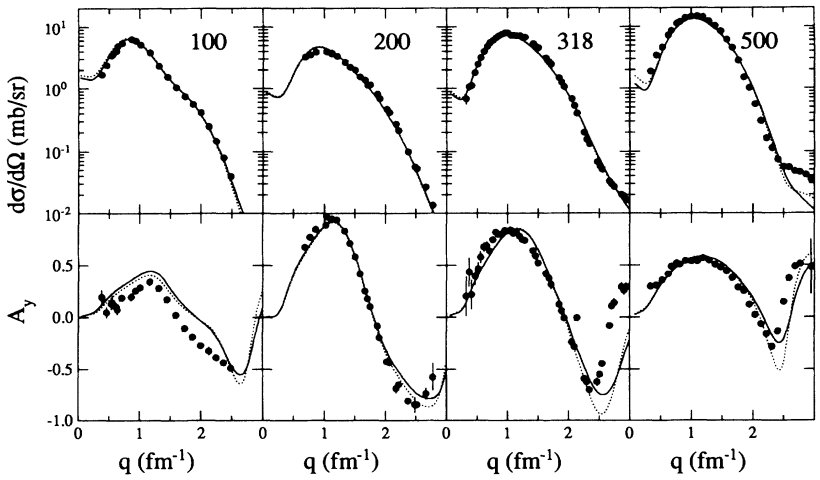


FIG. 3. Energy dependence of reaction models of $^9$Be$(p,p')\frac{5}{2}^-$ for $100 \leq E_p \leq 500$ MeV. Dotted curves portray DWBA and solid curves CC calculations.

power data, but has relatively little effect upon inelastic scattering. The principal effect of channel coupling upon the inelastic scattering calculations is damping of the analyzing power for large momentum transfer. This effect is about twice as strong for the $\frac{7}{2}^-$ state as for the $\frac{5}{2}^-$ state and increases with energy between 200 and 500 MeV. Also note that agreement with the elastic cross section data could be improved at all energies by shifting the monopole angular distribution toward smaller momentum transfer, as might be expected from the likely difference between neutron and proton densities for this nucleus. Hence, this energy-independent discrepancy is more likely due to inaccuracies in the structure model than in the reaction model.

For all energies we find that the quadrupole contribution to the elastic cross section is very important for momentum transfers larger than about 1.2 fm$^{-1}$ and is dominant near 1.7 fm$^{-1}$. The difference in the phase of the monopole and quadrupole analyzing-power oscillations dramatically damps the elastic analyzing power. The $A_y$ oscillation in the monopole calculations between 1.5 and 2.0 fm$^{-1}$ becomes markedly sharper between 200 and 500 MeV, but the data become much flatter. Both the magnitude and the energy dependence of this effect are nicely explained by the quadrupole contribution. The first negative dip in the monopole $A_y$ is associated with the node in the elementary analyzing power, occurs slightly before 1.5 fm$^{-1}$ near 100 MeV, and moves slowly toward larger momentum transfer as the energy increases. The next positive peak in $A_y$ is associated with the node in the monopole form factor which occurs at about 2.0 fm$^{-1}$ and hence its location is relatively constant with respect to energy. As the dip approaches the peak, the oscillation in $A_y$ becomes progressively sharper until a remarkable, almost singular, structure is obtained in the monopole analyzing-power calculation near 500 MeV. By contrast, the angular distribution of the quadrupole contribution, as exemplified by the $\frac{5}{2}^-$ angular distribution, displays a broad positive maximum centered near 1.2 fm$^{-1}$ followed by a negative maximum near 2.5 fm$^{-1}$, such that the competition between these two contributions conspires to produce a small and relatively flat analyzing-power angular distribution for $q > 1.5$ fm$^{-1}$. The positive maximum in the quadrupole $A_y$ fills in the negative dip in the monopole $A_y$, while the negative quadrupole maximum erases the next positive monopole peak. At higher energies the monopole $A_y$ for $q > 2.5$ fm$^{-1}$ is again going negative just where the quadrupole contribution goes

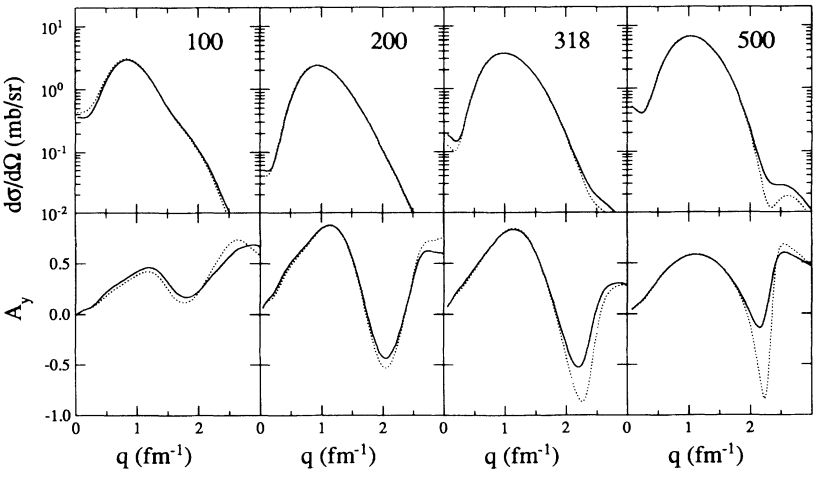


FIG. 4. Energy dependence of reaction models of $^9$Be$(p,p')\frac{7}{2}^-$ for $100 \leq E_p \leq 500$ MeV. Dotted curves portray DWBA and solid curves CC calculations.

positive and again damping of $A_y$ is obtained.

Also notice that at 500 MeV the cross section data for the $\frac{5}{2}^-$ state suggest a secondary peak at large momentum transfer. Such a peak could be due to a second maximum in either the proton or neutron form factors and is not excluded by the available electromagnetic data. If such a peak were present, it could cause the analyzing power to rise more rapidly for $q > 2.5$ fm$^{-1}$ and would probably improve the agreement with both the inelastic and elastic data.

### C. Effective interaction

Elastic and inelastic scattering calculations which illustrate the sensitivity to the density dependence of the effective interaction are presented in Figs. 5 and 6, where the dashed curves are based upon the Franey-Love $t$ matrix [31] (FL), the dotted curves use effective interactions based upon the theory of nuclear matter, and the solid curves employ empirical effective interactions (EI) fitted to proton scattering data for $A = 16$–$40$. For $E_p < 200$ MeV the dotted curves are based on the Paris-Hamburg $G$ matrix [8, 9] (PH), whereas for $E_p \geq 200$ MeV results based upon the LR interaction due to Ray [10] are shown. In all cases the same interactions were used to generate both the distorting and transition potentials.

These results clearly demonstrate the importance of medium modifications to the effective interaction. The $t$-matrix calculations are quite poor at all energies, even for 500 MeV. At 100 MeV the elastic and forward-angle inelastic cross section calculations are too large and the strongly positive analyzing-power calculations display none of the structure present in the data. The FL calculations for inelastic cross sections would have been even larger at low $q$ had a more realistic model of absorption, such as a standard phenomenological optical potential, been used. For larger momentum transfer the inelastic cross section falls below the data in a manner already familiar for normal-parity isoscalar excitations of self-conjugate targets using protons in the energy range $100 \leq E_p \leq 200$ MeV [1]. Similar problems with the $t$-matrix calculations are also observed at 200 MeV, except that the $A_y$ calculations, while still too positive, are begining to follow the angular distribution of the data more closely. Significant but insufficient improvements are obtained using the density dependence of the PH or LR interactions, but the low-$q$ cross sections remain substantially too large, especially at 200 MeV. Similar results at $E_p = 200$ MeV using the PH interaction in DWBA calculations for $^{6,7}$Li were obtained by Glover *et al.* [14, 15] and for $^{10}$B by Lewis *et al.* [16]. The deficiencies in the PH and LR calculations for $100 \leq E_p \leq 200$ MeV strongly resemble those already observed [25] for normal-parity excitations in $^{16}$O and $^{40}$Ca, for example, suggesting a common problem with the effective interaction.

Calculations using the empirical effective interactions fitted to data for $^{16}$O and $^{40}$Ca provide much better agreement with the data for $^{9}$Be than do the theoretical interactions, and the small remaining differences between calculations, and data are quite similar for all three targets. The consistency between CC calculations for $^{9}$Be and DWBA calculations for $^{16}$O and $^{40}$Ca supports the essential validity of the local density approximation even though the theoretical interactions are not yet sufficiently accurate to quantitatively reproduce the data. Although medium modifications of the effective interaction are quite strong, any dependence upon specific properties of individual nuclei beyond their density distributions appears to be minimal. To a good approximation the effective interaction appears to depend primarily upon local density and to be almost independent of nucleus, state, or deformation. However, for $100 \leq E_p \leq 200$ MeV we found that accurate fits to inelastic scattering data for states with surface-peaked transition densities require modification of the effective interaction even as the density approaches zero. We suggested the interpretation that corrections to the local density approximation for finite nuclei would enhance the medium modifications for low density and reduce them at high density with respect to infinite nuclear matter at the corresponding lo-

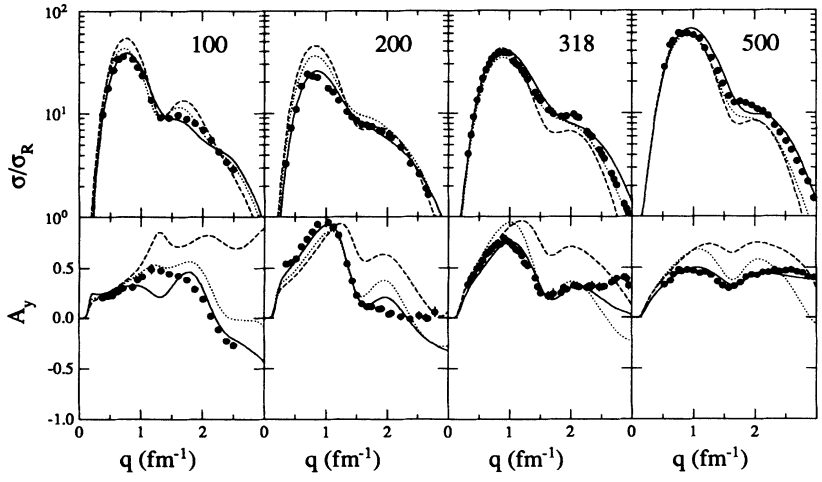


FIG. 5. Dependence of CC calculations for $^{9}$Be$(p,p')\frac{3}{2}^-$ upon medium modifications of the effective interaction. Dashed curves employ the FL $t$ matrix, dotted curves either the PH ($E_p < 200$ MeV) or the LR ($E_p \geq 200$ MeV) interactions, and solid curves empirical effective interactions.

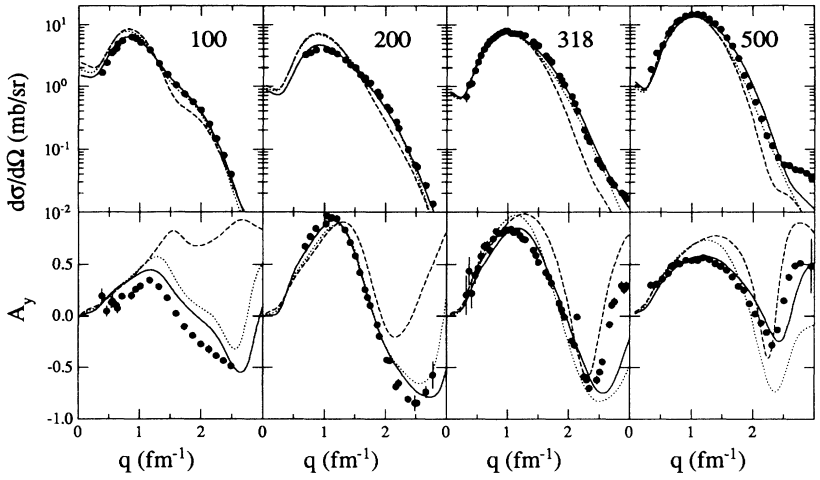


FIG. 6. Dependence of CC calculations for $^9$Be$(p,p')\frac{5}{2}^-$ upon medium modifications of the effective interaction. Dashed curves employ the FL $t$ matrix, dotted curves either the PH ($E_p < 200$ MeV) or the LR ($E_p \geq 200$ MeV) interactions, and solid curves empirical effective interactions.

cal densities [11]. The same effect is also observed for inelastic scattering by $^9$Be, for which a reduction in the interaction strength at low densities is required to reproduce the peak cross section. Evidently this effect does not depend strongly upon nuclear species either and can be incorporated within the local density approximation by suitable modification of the low-density limit of the effective interaction.

The oscillatory structure in elastic analyzing power develops rapidly as the energy increases above 100 MeV. In Fig. 7 we compare calculations using the FL, PH, and EI interactions with the data for $E_p = 135$ MeV. Note that the reaction model has been refined considerably since the original analysis of these data was made in Ref. [12] and the results are correspondingly improved. For elastic scattering we observe that the low-$q$ peak in the monopole $A_y$ distribution is already much more sharply defined than at 100 MeV. In fact, the data display a stronger peak at this energy than does the EI calculation. This deficiency in the empirical effective interaction was also observed for $^{16}$O at 135 MeV [11] and for $^{16}$O and $^{40}$Ca at 100 MeV [25]. The elastic scattering calculations for $^{16}$O using the EI interactions, which were fitted to inelastic scattering data alone, suppress the cross section too strongly near 1.5 fm$^{-1}$ and give too little analyzing power at low $q$. For this energy the PH interaction gives better agreement with the elastic scattering data, whereas the empirical interaction gives better agreement with the inelastic scattering data. Similar effects are also observed in $^9$Be for 100 and 135 MeV. The EI interaction gives a better description of the inelastic data and of the elastic analyzing power in the region of momentum transfer dominated by the quadrupole contribution, while the PH interaction gives a better description of the low-$q$ elastic analyzing power dominated by the monopole contribution. This apparent $A$-independent inconsistency between the elastic and inelastic scattering calculations for $E_p \leq 135$ MeV is probably related to an inaccuracy in the $(1 + \rho\partial/\partial\rho)$ rearrangement relationship between the elastic and inelastic interactions. Pauli blocking corrections are so large at low energies that higher-order terms may be required in the rearrangement relationship. Better self-consistency is obtained as the energy increases.

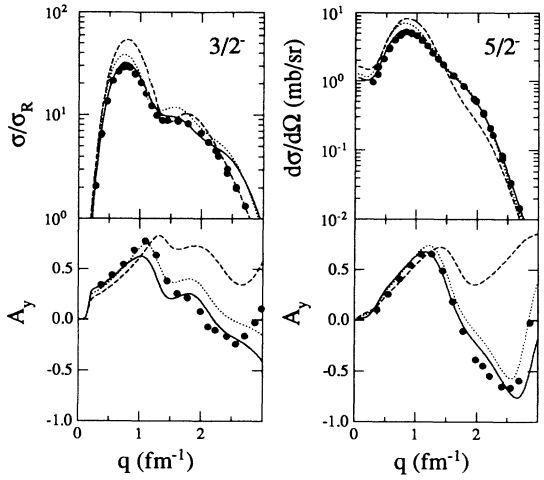


FIG. 7. Calculations for $^9$Be$(p,p')$ at $E_p = 135$ MeV using the FL (dashed lines), PH (dotted lines), and empirical effective interaction (solid lines).

## V. SUMMARY AND CONCLUSIONS

We have performed microscopic coupled-channels calculations for excitation of the $^9$Be ground-state rotational band by the $^9$Be$(p,p')$ reaction in the energy range $100 \leq E_p \leq 500$ MeV using transition potentials constructed by folding density-dependent effective interactions with transition densities obtained either from electron scattering or from the shell model. Better results are obtained using the form factors fitted to electron scattering than with the shell-model densities, demonstrating the sensitivity to the radial densities. The quadrupole contribution to elastic scattering from this severely deformed nucleus is particularly important, enhancing the cross section and damping the analyzing power for $q > 1.2$ fm$^{-1}$. These effects are described relatively accurately in DWBA, but higher-order contributions become more important as the interaction strength increases. These

higher-order contributions decrease between 100 and 200 MeV and then increase for larger energies. The higher-order contributions are also more important for the $\frac{7}{2}^-$ state than for the $\frac{5}{2}^-$ state.

The results also clearly demonstrate the importance of medium modifications to the effective interaction. LDA calculations based upon effective interactions for nuclear matter provide much better agreement with the data than do calculations using density-independent $t$ matrices. The best agreement is obtained using empirical effective interactions previously fitted to proton scattering data for $^{16}$O or $^{40}$Ca. The accuracy of CC calculations based upon the LDA is quite remarkable for a nucleus as small and as deformed as $^{9}$Be. Even the remaining discrepancies between calculations and data for $^{9}$Be are similar to those for heavier spherical nuclei. Therefore, medium modifications of the two-nucleon effective interaction depend primarily upon local density and are almost independent of nucleus, state, or deformation.

The present results for $^{9}$Be and the previous results for $^{16}$O and $^{40}$Ca all require modification of the effective interaction even as the local density approaches zero, suggesting that an extension of the local density approximation is required for finite nuclei. Although it is plausible that medium modifications to the effective interaction in finite nuclei are larger at low density and smaller at high density than in infinite nuclear matter with the corresponding densities, further theoretical work is needed to clarify this issue. It also appears that the first-order rearrangement relationship between elastic and inelastic interactions needs refinement for energies below about 135 MeV. For lower energies the Pauli blocking corrections are so large that an apparent inconsistency between the interactions that give the best fits to elastic and inelastic scattering data separately probably reflects inaccuracy in the rearrangement relationship. This problem, and the lack of detailed effective interactions below 100 MeV, appears to limit the applicability of the present model to energies above 100 MeV.

## ACKNOWLEDGMENTS

We would like to thank Dr. D.J. Millener for providing the spectroscopic amplitudes for Cohen and Kurath wave functions. We also thank Prof. H.P. Blok, Dr. G. van der Steenhoven, L.J. de Bever, and J. Blouw for inspiring this project with their work on $^{10}$B$(e,e'p)$ and $^{10}$B$(\gamma,p)$. Finally, the hospitality of NIKHEF-K is gratefully acknowledged. Support for this work has been provided by the Foundation for Fundamental Research of Matter (FOM) in The Netherlands and by the U.S. National Science Foundation.

[1] J.J. Kelly, W. Bertozzi, T.N. Buti, F.W. Hersman, C. Hyde, M.V. Hynes, B.E. Norum, F.N. Rad, A.D. Bacher, G.T. Emery, C.C. Foster, W.P. Jones, D.W. Miller, B.L. Berman, W.G. Love, and F. Petrovich, Phys. Rev. Lett. **45**, 2012 (1980).

[2] J.J. Kelly, W. Bertozzi, T.N. Buti, J.M. Finn, F.W. Hersman, C. Hyde-Wright, M.V. Hynes, M.A. Kovash, B. Murdock, B.E. Norum, B. Pugh, F.N. Rad, A.D. Bacher, G.T. Emery, C.C. Foster, W.P. Jones, D.W. Miller, B.L. Berman, W.G. Love, J.A. Carr, and F. Petrovich, Phys. Rev. C **39**, 1222 (1989).

[3] J.J. Kelly, J.M. Finn, W. Bertozzi, T.N. Buti, F.W. Hersman, C. Hyde-Wright, M.V. Hynes, M.A. Kovash, B. Murdock, P. Ulmer, A.D. Bacher, G.T. Emery, C.C. Foster, W.P. Jones, D.W. Miller, and B.L. Berman, Phys. Rev. C **41**, 2504 (1990).

[4] Q. Chen, J.J. Kelly, P.P. Singh, M.C. Radhakrishna, W.P. Jones, and H. Nann, Phys. Rev. C **41**, 2514 (1990).

[5] J.J. Kelly, A.E. Feldman, B.S. Flanders, H. Seifert, D. Lopiano, B. Aas, A. Azizi, G. Igo, G. Weston, C. Whitten, A. Wong, M.V. Hynes, J. McClelland, W. Bertozzi, J.M. Finn, C.E. Hyde-Wright, R.W. Lourie, P.E. Ulmer, B.E. Norum, and B.L. Berman, Phys. Rev. C **43**, 1272 (1991).

[6] J.J. Kelly, P. Boberg, A.E. Feldman, B.S. Flanders, M.A. Khandaker, S.D. Hyman, H. Seifert, P. Karen, B.E. Norum, P. Welch, S. Nanda, and A. Saha, Phys. Rev. C **44**, 2602 (1991).

[7] B.S. Flanders, J.J. Kelly, H. Seifert, D. Lopiano, B. Aas, G. Igo, G. Weston, A. Wong, M.V. Hynes, J. McClelland, W. Bertozzi, J.M. Finn, C.E. Hyde-Wright, R.W. Lourie, B.E. Norum, P. Ulmer, and B.L. Berman, Phys. Rev. C **43**, 2103 (1991).

[8] H.V. von Geramb, in *The Interaction between Medium Energy Nucleons in Nuclei - 1982*, Proceedings of the Workshop on the Interactions between Medium Energy Nucleons in Nuclei, edited by Hans-Otto Meyer, AIP Conf. Proc. No. 97 (AIP, New York, 1983), p. 44.

[9] L. Rikus, K. Nakano, and H.V. von Geramb, Nucl. Phys. **A414**, 413 (1984).

[10] L. Ray, Phys. Rev. C **41**, 2816 (1990).

[11] J.J. Kelly, Phys. Rev. C **39**, 2120 (1989).

[12] J.J. Kelly, Phys. Rev. C **38**, 1490 (1988).

[13] S. Dixit, W. Bertozzi, J.M. Finn, F.W. Hersman, C.E. Hyde-Wright, M.V. Hynes, M.A. Kovash, B.E. Norum, J.J. Kelly, A.D. Bacher, G.T. Emery, C.C. Foster, W.P. Jones, D.W. Miller, B.L. Berman, and D.J. Millener, Phys. Rev. C **43**, 1758 (1991). Note that Table II contains a typographical error: The LGE coefficient $a_1$ for $\rho_p$ for the $\frac{5}{2}^-$ state should be $-1.262 \times 10^{-2}$.

[14] C.W. Glover, C.C. Foster, P. Schwandt, J.R. Comfort, J. Rapaport, T.N. Taddeucci, D. Wang, G.J. Wagner, J. Seubert, A.W. Carpenter, J.A. Carr, F. Petrovich, R.J. Philpott, and M.J. Threapleton, Phys. Rev. C **41**, 2487 (1990).

[15] C.W. Glover, C.C. Foster, P. Schwandt, J.R. Comfort, J. Rapaport, T.N. Taddeucci, D. Wang, G.J. Wagner, J. Seubert, A.W. Carpenter, J.A. Carr, F. Petrovich, R.J. Philpott, and M.J. Threapleton, Phys. Rev. C **43**, 1664 (1991).

[16] P.R. Lewis, G.G. Shute, B.M. Spicer, R.S. Henderson, R. Abegg, D. Frekkers, O. Häusser, K.P. Jackson, C.A. Miller, and S. Yen, Nucl. Phys. **A532**, 583 (1991).

[17] T. Tamura, Rev. Mod. Phys. **37**, 679 (1965).

[18] J. Raynal, Centre d'Études Nucléaires de Saclay Report No. IAEA-SMR-9/8, 1972.
[19] G. Roy, H.S. Sherif, E.D. Cooper, L.G. Greeniaus, G.A. Moss, J. Soukup, G.M. Stinson, R. Abegg, D.P. Gurd, D.A. Hutcheon, R. Liljestrand, and C.A. Miller, Nucl. Phys. **A442**, 686 (1985).
[20] V.O. Nesterenko, I.N. Kukhtina, A.V. Sushkov, and D.T. Khoa, J. Phys. G **14**, 725 (1988).
[21] G. Bertsch, J. Borysowicz, H. McManus, and W.G. Love, Nucl. Phys. **A284**, 399 (1977).
[22] J.J.A. Zalmstra, M.N. Harakeh, and J.F.A. van Hienen, Nucl. Phys. **A535**, 23 (1991).
[23] J.P. Jeukenne, A. Lejeune, and C. Mahaux, Phys. Rev. C **16**, 80 (1977).
[24] J.P. Glickman, W. Bertozzi, T.N. Buti, S. Dixit, F.W. Hersman, C.E. Hyde-Wright, M.V. Hynes, R.W. Lourie, B.E. Norum, J.J. Kelly, B.L. Berman, and D.J. Millener, Phys. Rev. C **43**, 1740 (1991).
[25] H. Seifert, Ph.D. thesis, University of Maryland, 1990.
[26] D. Lopiano, draft Ph.D. thesis, UCLA, 1983.
[27] F. Petrovich, R.J. Philpott, A.W. Carpenter, and J.A. Carr, Nucl. Phys. **A425**, 609 (1984).
[28] S. Cohen and D. Kurath, Nucl. Phys. **73**, 1 (1965).
[29] D.J. Millener, private communication.
[30] R.S. Hicks, J. Button-Shafer, B. Debebe, J. Dubach, A. Hotta, R.L. Huffman, R.A. Lindgren, G.A. Peterson, R.P. Singhal, and C.W. de Jager, Phys. Rev. Lett. **60**, 905 (1988).
[31] M.A. Franey and W.G. Love, Phys. Rev. C **31**, 488 (1985).
[32] T. Cheon, K. Takayanagi, and K. Yazaki, Nucl. Phys. **A437**, 301 (1985).
[33] T. Cheon, K. Takayanagi, and K. Yazaki, Nucl. Phys. **A445**, 227 (1985).
[34] J.J. Kelly, computer program LEA (unpublished).
[35] J. Raynal, computer program ECIS79 (unpublished).